Penerbit Akademia Baru

Journal of Advanced Research in Fluid Mechanics and Thermal Sciences

Journal homepage: www.akademiabaru.com/arfmts.html
ISSN: 2289-7879

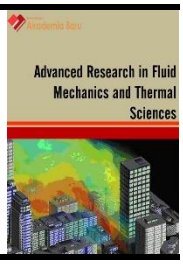

Numerical Investigation of Drag Force on Micro-sized Magnetic Beads in Microchannel with Chamber Design

Open Access

Muhammad Asnawi Vaea[1], Ummikalsom Abidin[1,*], Natrah Kamaruzaman[1], Fazila Mohd Zawawi[1], Muhammad Noor Afiq Witri Muhammad Yazid[1]

[1] Department of Thermofluids Engineering, School of Mecahnical Engineering, Faculty of Engineering, Universiti Teknologi Malaysia, 81310 Skudai, Johor, Malaysia

ARTICLE INFO

Article history:
Received 13 September 2018
Received in revised form 29 November 2018
Accepted 6 December 2018
Available online 16 May 2019

ABSTRACT

Biological cells or bioparticles separation is a primary step in most biological studies. One of the microfluidic bioparticles separation methods is the magnetic-based method. Integrated microfluidic magnetic bioparticle separation device is made up of a microfluidics channel and a magnetic system. From past studies, the design of the microfluidic channel is least discussed in comparison with the magnetic system. To fill this gap, this study has focused on numerical simulation of a microfluidic channel with chamber design and the drag forces experienced by the magnetic beads. Simulation of the microfluidics channel was done with ANSYS Fluent software. The width ratios of trapping chamber and main channel ranged from 1 to 20, the flow rates ranged from 1 µL/min to 100 µL/min, and the bead sizes ranged from 5 µm to 25 µm were used in the numerical investigation. It was discovered that as the width ratio between the trapping chamber and main channel increases, the maximum velocity decreases, causing the Reynold's number to decrease. The pressure drop become greater at higher flow rate. Higher width ratio caused the drag force to reduce at a constant microbead size. At a constant width ratio between the trapping chamber and main channel, larger microbead sizes caused larger drag force. The microfluidic system with width ratio of 20 and flow rate of 1 µL/min produced the lowest drag force, 3.64 x 10^4 pN. Since particle trapping would occur when the magnetic force is larger than the drag force, therefore a high gradient magnetic system which offered high magnetic force was proposed to be integrated with the microfluidics system.

Keywords:
Drag force, micro-sized bead, flow rate, microchannel, trapping chamber, microfluidics

1. Introduction

Due to existence of severe diseases such as acquired immune deficiency syndrome (AIDS), cancer, and malaria, organizations all around the globe are carrying out various researches to seek for better solutions on this matter. According to Bhagat *et al.,* [2], the separation and concentration of rare cells for sample preparation process are the primary step in most biological studies, such as disease

* *Corresponding author.*
E-mail address: ummi@utm.my (Ummikalsom Abidin)

diagnosis. Standard techniques for cells sorting and separation include processing steps of filtration, centrifugation and sedimentation [3]. However, there are situations in which the cell size or density differences are not significant. In this context, microfluidic lab-on-chip (LOC) devices are widely applied.

Microfluidic particles separation methods can be categorized into active and passive techniques. Active techniques depend on an external force field for functionality, while passive techniques which depend entirely on the channel geometry and inherent hydrodynamic forces to function [2][4]. Magnetic separation method falls under the category of active techniques. Due to its non-contact nature, magnetic separation can maintain the cell viability and suit well with biological investigations [5].

Microfluidic magnetic particle separation device is made up of microfluidic channel and magnetic system. Over the years, to further develop this technology, researchers all around the worlds keep on studying on how the magnetic system might be further optimized to directly develop this microfluidic magnetic cell separation technique. However, not many papers can be found which discussed about the design of the microfluidic channel itself. Most of the studies only utilized cylindrical-shaped or flat-shaped microchannels in their researches, without the application of chamber as a trapping section. Studies by Teste *et al.,* [6] and Pamme and Wilhelm [7] applied chamber design in their microfluidic channels, however their studies emphasized more on the development of the magnetic system, not on the design of the microfluidic channel.

To fill this gap, this study, which utilized a chamber design in the microfluidic channel was carried out to investigate the drag forces experienced by micro-sized magnetic beads and to determine the possibility of beads trapping with magnetic system application. Different widths of trapping chamber were applied and the resulting effects on drag forces experienced by the beads were investigated. The width of main channel was kept constant at 100 µm, thus higher width of trapping chamber produced higher width ratio (*WR*) between the trapping chamber and main channel. The total length of the developed microfluidic channel was 14 000 µm with height of 100 µm. The width ratios ranged from 1 to 20, the flow rates ranged from 1 to 100 µL/min, and the bead sizes ranged from 5 µm to 25 µm. Three-dimensional models were developed using ANSYS Fluent software. Beads trapping would occur when magnetic force is larger than drag force. By referring to the generated drag force, appropriate magnetic system which would enable beads trapping was proposed.

2. Theoretical

Theoretical relationships were required to validate data during pre-simulation study and to acquire data of the drag forces. The geometry of the microfluidic channel model during pre-simulation study followed a rectangular geometry. In a paper by Fuerstman *et al.,* [8], they stated that in a rectangular channel without the presence of bubbles or obstructions, the laminar flow of a single liquid phase through the channel approximately follows Eq. (1).

$$\Delta P = \frac{a\eta QL}{WH^3} \tag{1}$$

In which,

$$a = 12[1 - \frac{192H}{\pi^5}\tanh\left(\frac{\pi W}{2H}\right)]^{-1} \tag{2}$$

where ΔP is pressure drop between two points, η is the fluid viscosity, Q as volumetric flow rate, L represents the length of microchannel, W as width of microchannel, and H as height of microchannel. Eq. (1) is accurate to within 0.26% for any rectangular channel that has $W/H < 1$ and Reynold's number < ~1000. To investigate the relationship between volumetric flow rate, Q, average fluid velocity, u_{ave}, and cross-sectional area, A, the following equation was applied.

$$Q = u_{ave}A \tag{3}$$

As this fluid was assumed flowing under laminar condition, the value of the theoretical maximum fluid velocity for comparison with the simulated values during pre-simulation study could be calculated by doubling the value of average fluid velocity

$$u_{max} = 2u_{ave} \tag{4}$$

$$u_{max} = 2\frac{Q}{A} \tag{5}$$

The acquired u_{ave} was applied to obtain Reynold's number, Re while u_{ave} was utilized in calculations of drag force. Utilizing the equation as applied by Di Carlo [9], the Reynold's numbers were calculated using the relationship

$$Re = \frac{\rho u_{ave} L_c}{\eta} \tag{6}$$

where ρ is fluid density and L_c is the characteristic length. As the geometry of the microfluidic channel is rectangular, characteristic length, L_c, was represented by hydraulic diameter, d_h, where U is the wetted perimeter of the microfluidic channel in which

$$d_h = \frac{4A}{U} \tag{7}$$

Determining Re would validate the assumption of laminar flow as $Re < 2100$ represents laminar condition. In addition, the laminar entrance length, $Le_{laminar}$, which is the distance that a fluid travels after entering the channel to become fully developed in its flowing condition, could also be analyzed after determining the Reynold's number, as follows.

$$Le_{laminar} = 0.05(Re)(d_h) \tag{8}$$

Based on the papers by Hejazian *et al.,* [10], the following drag force relationship was applied throughout the study.

$$F_{drag} = 3\pi d_c u_{max} \tag{9}$$

where F_{drag} represents drag force experienced by the micro-sized magnetic beads and d_c is the diameter of the beads. Ultimately, trapping would occur when the generated magnetic force, $F_{magnetic}$ is larger than F_{drag}.

3. Methodology

3.1 Numerical Simulation

Before proceeding to the Grid Independence Test and theoretical comparison for the model in this study, a microfluidic channel with chamber design of a previous research [1] was first developed using ANSYS Fluent and studied through the solving of Navier-Stokes by the software as the dimensions of this model is almost similar to the investigated dimensions in this research. Although the trapping concept is similar, the main objective of the past numerical research was to study on the magnetic system whereby this research was to investigate the effects of the dimensions of the trapping chamber. This procedure was required to ensure that this research was conducted with better understandings on the establishment of boundary conditions and fluid model of the simulation studies.

The length of the whole system was 14000 µm, the height was 110 µm with width of 300 µm. The diameter of the trapping chamber was 750 µm. The flowing fluid was modelled as water at 25 °C, with density of 997.13 kg/m^3 and dynamic viscosity of 0.891 x 10^{-3} Pa-s. The obtained values of the ANSYS Fluent simulation were then compared with the available data from the past study, as in Table 1.

Table 1
Comparison between past study's and simulated data

	Q = 1 µL/min		*Q* = 10 µL/min		*Q* = 100 µL/min	
	$u_{max}, m/s$	*ΔP, Pa*	$u_{max}, m/s$	*ΔP, Pa*	$u_{max}, m/s$	*ΔP, Pa*
Past Study	4.04 x 10^{-4}	8.12	4.04 x 10^{-3}	Not	4.04 x 10^{-2}	Not
Simulated	4.06 x 10^{-4}	7.89	4.04 x 10^{-3}	available	4.14 x 10^{-2}	available
Difference	0.50 %	2.83%	0.50%		2.48%	

The calculated maximum velocity values were the ones in the middle of the trapping chamber while the pressure drop was measured between the inlet and the outlet of the microfluidic channel. Thus, as the differences between the past study's data and simulated data were very low, as the maximum difference was only 2.83%, the understandings of the boundary conditions and fluid model of the simulation studies were verified. Therefore, the research was then continued with the simulation of the models which were to be investigated in this research.

3.1.1 Assumptions, limitations and boundary conditions

One of the main assumptions in this research was that the flowing fluid in the microfluidic channel exhibited diluted blood rheological properties, thus assumed as incompressible Newtonian fluid with viscosity of 0.00096 Pa-s and density of 1027 kg/m^3, as applied by Wu *et al.,* [11]. The fluid was also assumed flowing under laminar condition in continuous flow. Continuous-flow separation has a high throughput with no limits on its capacity. In addition, it also possesses the possibility of continuous monitoring and adjusting the separation parameters, high potential for system integration, and lateral separation of sample components [10]. There are a few forces that acted upon the magnetic beads. However, according to Hejazian *et al.,* [10], many of the mentioned forces could be ignored for cell separation applications, depending on the particle sizes and the magnetic field strength magnitude. In addition, according to Gijs *et al*., [12] as well, in a relatively high magnetic field typically generated by permanent magnets, drag force and magnetic force are the most dominant forces, and the other forces could be ignored. Thus, only drag force and magnetic force were considered in this research. Besides that, another assumptions made were the inner part of the microfluidic channel

exhibited smooth surface conditions and the velocity of the micromagnetic beads was similar as the velocity of the flowing fluid.

Flow rate as high as 1000 microliter/min was not to be applied as the high shearing effect could damage the flowing particle and since the fluid flowing for active microfluidic cells and particles separation typically slow, the maximum flow rate applied in this experiment was 100 microliter/minute. No flow rate lesser than 1 microliter/minute was used as it is too slow and not suitable for future experimental purposes. Typically, the syringe pump would be controlled to adjust the fluid flow rates accordingly in experiments. Besides that, for Polydimethylsiloxane (PDMS)-based device, according to Qin, Xia, and Whitesides [13], using too wide channels (height to width ratio < 0.05) can cause sagging of the top layer under its own weight or excessive flow pressure. Thus, since the width of the main channel to be maintained at 100 micrometer, the largest width of the trapping chamber should be lower than 2000 micrometer (2 millimeter). Therefore, considering 2000 micrometer as the maximum trapping chamber width, the width ratio of trapping chamber to main channel ranges from 1 to 20. In addition, the sizes of the micromagnetic particle used were ranging from 5 µm to 25 µm, as that range of sizes is very typical for rare cells, such as cancer cells [14,15].

The input flow rate were specified at the inlet of the microfluidic channel while the pressure outlet boundary conditions were specified at the other end as the fluid was flowing in the direction of the x-axis. The input volumetric flow rate should be ranging from 1 µL/minute to 100 µL/minute. The outlet pressure was set to be 0 gauge pressure. A no-slip boundary condition was set on the walls of the microfluidic channel model.

3.1.2 Grid independence test and theoretical comparisons

For Grid Independence Test, a three-dimensional simulation model with width ratio of 1 was developed using ANSYS Fluent. Up to three runs were conducted. The maximum velocities between the runs did not differ much as the highest percentage difference was only 0.54%. The maximum velocity values were already almost fully converging with each other as early as Run 2. However, for the pressure drop, the maximum percentage difference between Run 1 and Run 2 was as much as 10.75%, as visualized in Figure 1. Another run, which was Run 3 was carried out and the pressure drop values further converged, causing maximum percentage difference between Run 2 and Run 3 dropped to 3.18% only. Therefore, the meshing refinement settings as in Run 2, with 139 000 elements for *WR* of 1, was chosen as the most optimum setup of meshing.

Besides, the simulated data had also been compared with the data obtained through theoretical relationship. Eq. (1) and (5) were utilized to obtain theoretical values of maximum velocities and pressure drops. The theoretical values are presented in Table 2.

Comparison between the simulated maximum velocities and the theoretical maximum velocities for width ratio of 1 yielded percentage difference up to only 0.24%. Besides that, the comparisons for pressure drops gave maximum percentage difference of only 2.86% and both the theoretical and simulated pressure drops exhibits similar patterns when plotted against the flow rates, as shown in Figure 2.

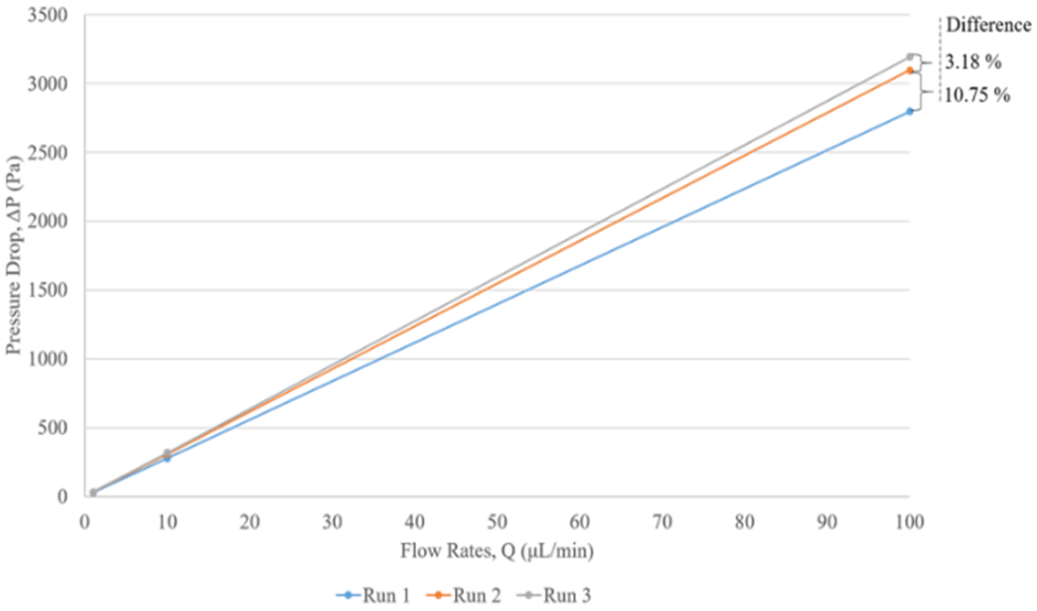

Fig. 1. Pressure drops of GIT for *WR* of 1

Table 2
Theoretical *ΔP* and u_{max} for *WR* of 1

Theoretical pressure drops, ΔP (Pa) according to flow rates (μL/min)			Theoretical maximum velocities, $\mathbf{u_{max}}$ (m/s) according to flow rates (μL/min)		
1 μL/min	10 μL/min	100 μL/min	1 μL/min	10 μL/min	100 μL/min
63.3112	633.112	6331.12	0.003333	0.033333	0.333333

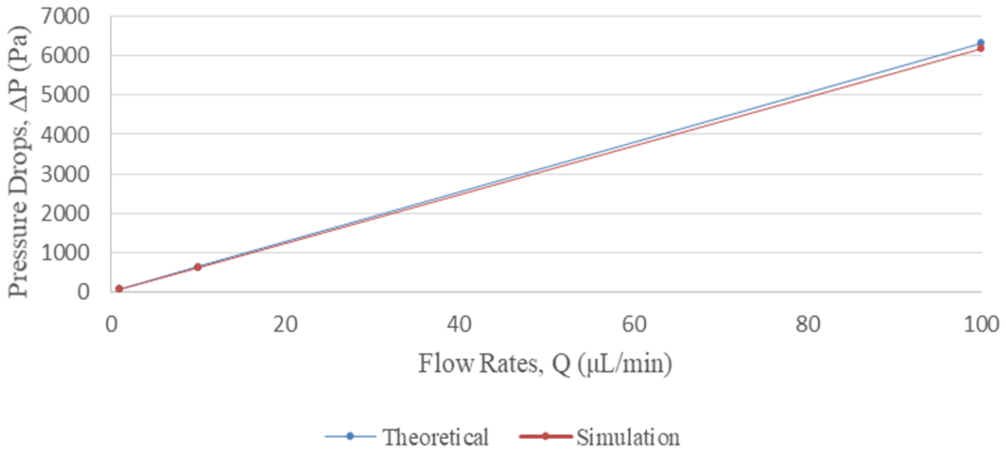

Fig. 2. Comparison of theoretical and simulated pressure drops for *WR* of 1

3.1.3 Meshing quality

Prior to running the simulations of the microfluidic channel with chamber design, the meshing quality of each of the three-dimensional models was appraised first. 11 different models were developed, with *WR* of 1, 2, 4, 6, 8, 10, 12, 14, 16, 18, and 20 respectively. The most minimum orthogonality quality, 0.21, most maximum orthogonality skewness, 0.67, and the highest maximum aspect ratio, 19.6, were exhibited by the model with *WR* of 14. Since all of the three-dimensional models exhibited orthogonality qualities higher than 0.20, orthogonality skewnesses lower than 0.80,

and aspect ratios lower than 100, which are the acceptable ranges according to ANSYS Fluent User's Guide version 15 [16], thus, the meshings of each model were reliable enough to be applied throughout the simulation phase of this research.

4. Results

4.1 Maximum Velocity, Reynold's Number and Entrance Length

Volumetric flow rate was utilized as input parameter in this research. The values applied were 1 µL/min, 20 µL/min, 40 µL/min, 60 µL/min, 80 µL/min, and 100 µL/min, which influenced the fluid velocity distributions of the model. The differences of the magnitudes of the velocities at the trapping chambers as the width ratio increases were visualized in Figure 3. As observed in the figure, for a straight channel (*WR* = 1), when the width ratio between the trapping chamber and main channel was the lowest, it gave the maximum velocity magnitude of 3.34 x 10^{-3} m/s. While for the microfluidic channel with trapping chamber design, at *WR* = 4, the maximum velocity was 9.18 x 10^{-4} m/s, followed by 4.24 x 10^{-4} m/s at *WR* = 8, 2.75 x 10^{-4} m/s at *WR* = 12, 2.03 x 10^{-4} m/s at *WR* = 16, and lastly 1.61 x 10^{-4} m/s at *WR* = 20, which was the lowest magnitude of maximum velocity. Therefore, it can be concluded that for fluid flowing at a constant flow rate, as the width ratio increases, the maximum velocity decreases. The reduction of maximum velocities as the *WR*s were being increased would really help to provide a more effective magnetic bead trapping scenario in the system.

As the fluid being applied in this simulation model was incompressible, thus similar amount of fluid must flow past any point in the microfluidics channel in a given time to ensure the continuity of the flow. Therefore, given that the applied flow rate was constant, as the cross-sectional area of the microfluidic channel increases, necessarily the velocity would decrease.

In addition, the generated maximum velocities due to varying inputs of flow rates at constant width ratio between the trapping chamber and main channel were also investigated. The magnitudes of the corresponding maximum velocities at a constant *WR* of 10 were visualized in Figure 4.

As shown in Figure 4, the lowest generated maximum velocity, 3.33 x 10^{-4} m/s was when the flow rate of 1 µL/min was applied. It was then followed by the flow rate of 20 µL/min with 6.67 x 10^{-3} m/s, flow rate of 60 µL/min with 2.03 x 10^{-2} m/s, and the highest generated maximum velocity, 3.51 x 10^{-2} m/s was from the flow rate of 100 µL/min. Thus, it may be concluded that at a constant width ratio between the trapping chamber and main channel, the maximum velocity generated increases as the flow rate increases.

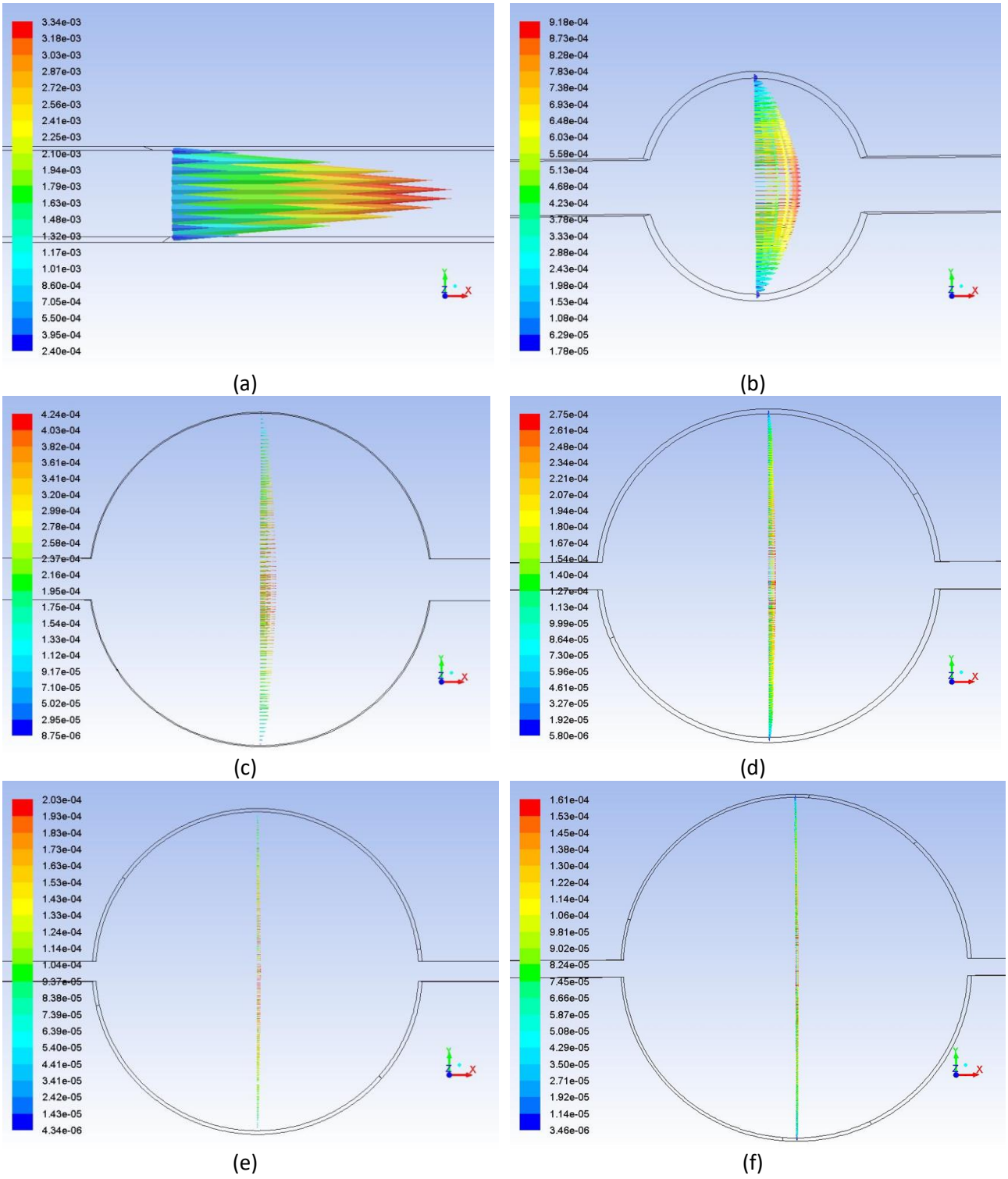

Fig. 3. Velocity in the trapping chamber at Q = 1 µL/min for *WR* of (a) 1, (b) 4, (c) 8, (d) 12, (e) 16, and (f) 20

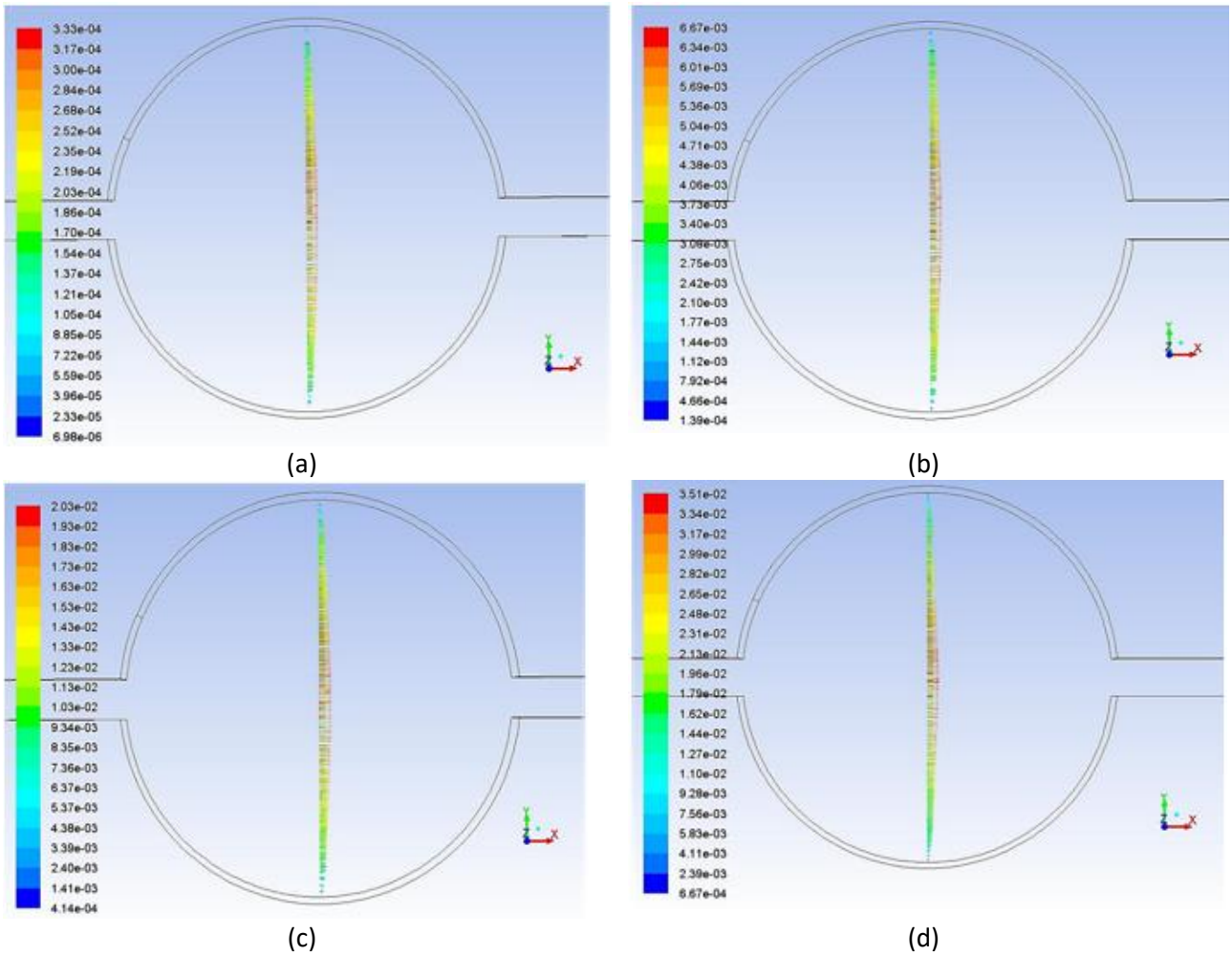

Fig. 4. Velocity in the trapping chamber at *WR* of 10 for flow rate of (a) 1 µL/min, (b) 20 µL/min, (c) 60 µL/min, and (d) 100 µL/min

By determining the velocity of the fluid flow, the Reynold's number can be calculated using Eq. (6). The maximum Reynold's number of the flowing fluid in the system was determined by considering the highest velocity of the fluid, 0.333333 m/s, which was in the simulation of *WR* = 1 with *Q* = 100 µL/min. Thus, by utilizing Eq. (6), it was discovered that the highest Reynold's number in the simulations was 17.83. Therefore, validating that the fluid flowing in the simulation was in laminar condition.

In addition, the entrance length could also be analyzed after determining the Reynold's number. As laminar flow condition was adopted, Eq. (8) was applied. The highest Reynold's number should give the furthest entrance length. With Reynold's number of 17.83, the corresponding entrance length is 89.15 µm. As the distance of entrance length was before entering the trapping chamber, thus it could be concluded that the fluid flowing inside the trapping chamber was fully-developed in laminar condition.

4.2 Pressure Drop

Investigating the parameter of pressure drop, *ΔP* was vital to determine the operational limit of a microfluidic channel. It must be ensured not to exceed the bonding strength between the surfaces of the microfluidic channel layers. Polydimethylsiloxane (PDMS) is a common raw material for the fabrication of microfluidic system [17-19]. PDMS layers can be adhered reversibly and irreversibly,

with regards to the techniques being applied. According to Anderson *et al*., [17], reversible methods are only appropriate for low pressure applications, which are lower than 35 kPa as the Van der Waals bonding is too weak. On the other hand, an irreversible bonding technique is able to handle relatively higher pressure, typically 100 kPa and above [20]. Therefore, the maximum pressure drop generated in this research needs to be determined to investigate the sustainability of the microfluidic channel system during real-life application.

The pressure drop that was being observed in this research was the pressure difference between the inlet and the outlet. Figure 5 shows the pressure contours for microfluidic channel model with WR of 10 and flow rates of (a) 1 µL/min (b) 20 µL/min (c) 60 µL/min, (d) 100 µL/min.

As being visualized in Figure 5, the pressure was maximum at the inlet and it kept on decreasing throughout the flow until it reached the value of 0 Pa at the outlet, which was one of the boundary conditions. Similar pattern of pressure contours would be observed in all of the simulation models. With *WR* of 10, flow rate of 1 µL/min caused pressure drop as much as 58.18 Pa. Besides that, the pressure drop was 1164 Pa for flow rate of 20 µL/min, 3500 Pa for flow rate of 60 µL/min, and 5847 Pa for flow rate of 100 µL/min. As the flow rate increases, the pressure drop increases.

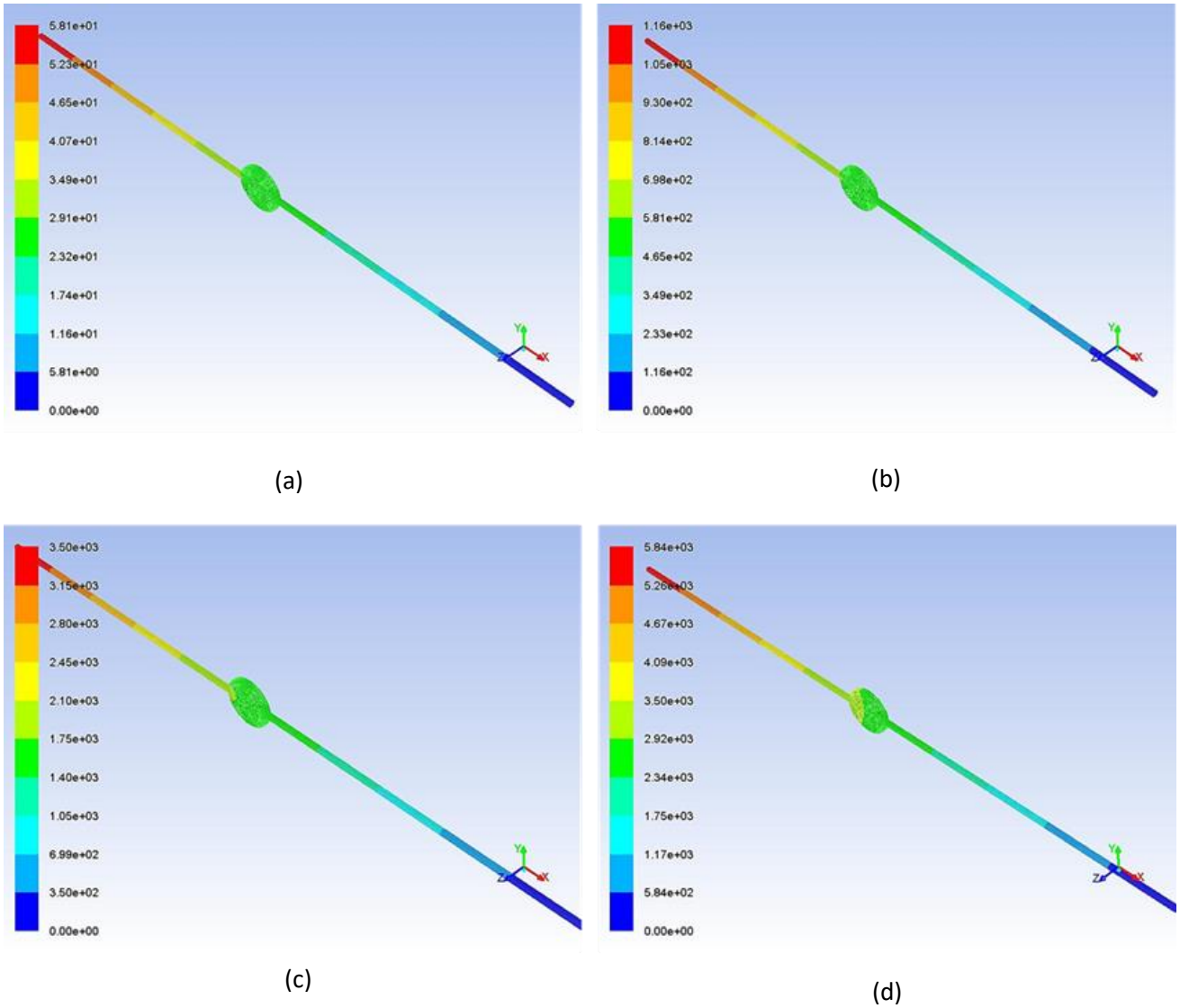

Fig. 5. Pressure contours at *WR* of 10 for flow rate of (a) 1 µL/min, (b) 20 µL/min, (c) 60 µL/min, and (d) 100 µL/min

Therefore, to determine the highest value of pressure drop in the simulation, the value of the highest volumetric flow rate, which was 100 µL/min must be considered, as well as the highest *WR* which gave the highest pressure drop. Figure 6 visualized the pressure contours at flow rate of 100 µL/min for the *WR*s of (a) 1, (b) 6, (c) 12, and (d) 20.

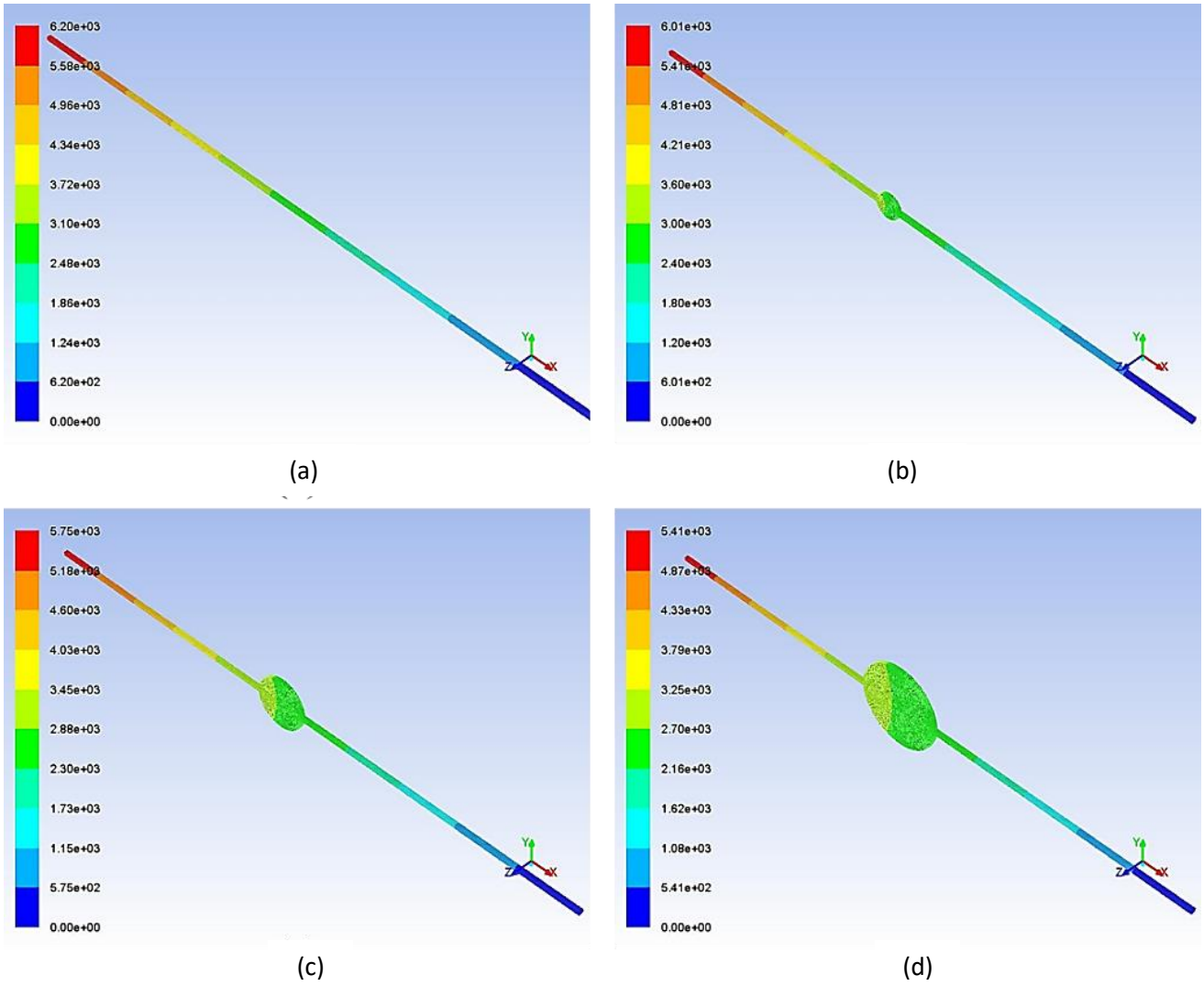

Fig. 6. Pressure contours at flow rate of 10 µL/min for *WR* of (a) 1, (b) 6, (c) 12, and (d) 20

From Figure 6, it can be observed that for *WR* of 1, the pressure drop was as high as 6206 Pa. It was 6016 Pa for *WR* of 6, 5761 Pa for *WR* of 12, and the lowest was 5417 Pa for investigated *WR* of 20. Thus, it can be concluded that as the width ratio between the trapping chamber and main channel increases, the pressure drop decreases.

Thus, the highest pressure drop that occured in the simulation could be found in the simulation with *WR* of 1 and flow rate of 100 µL/min, which was 6206 Pa. With the application of the microfluidic system which gave the maximum pressure drop, it still had not exceed the bonding strength between the surfaces of the PDMS microfluidic channel layers, which is maximum 35kPa for reversible technique and typically 100 kPa and higher for irreversible technique. Therefore, in real-life application, the microfluidic channel would be able to sustain itself.

4.3 Drag Force

The magnitudes of drag forces in the middle of the trapping chamber were numerically determined through Eq. (9). The applied values of the diameter of the magnetic bead were manipulated between 5 µm, 10 µm, 15 µm, 20 µm, and 25 µm. Figure 7 shows the relationship between the drag force and the flow rate at varying ratio of width between the trapping chamber and main channel. The bead size was kept constant at 5 µm. At *WR* of 20, when the flow rate applied was 1 µL/min, the resulting drag force in the trapping chamber was 7.28 x 10^3 pN, while flow rate of 100 µL/min yielded drag force of 7.36 x 10^5 pN. Drag force occurs as materials resist changes in velocity, thus as higher flow rate would produce higher velocity at a fixed area or area with small changes in size, thus higher drag force would be experienced. On the other hand, by analyzing the width ratio of trapping chamber and main channel at a constant flow rate, which was 100 µL/min, it was discovered that the highest drag force obtained, 3.81 x 10^6 pN was generated in the model with *WR* of 4, while the lowest drag force, 7.36 x 10^5 pN, was discovered in the model with *WR* of 20.

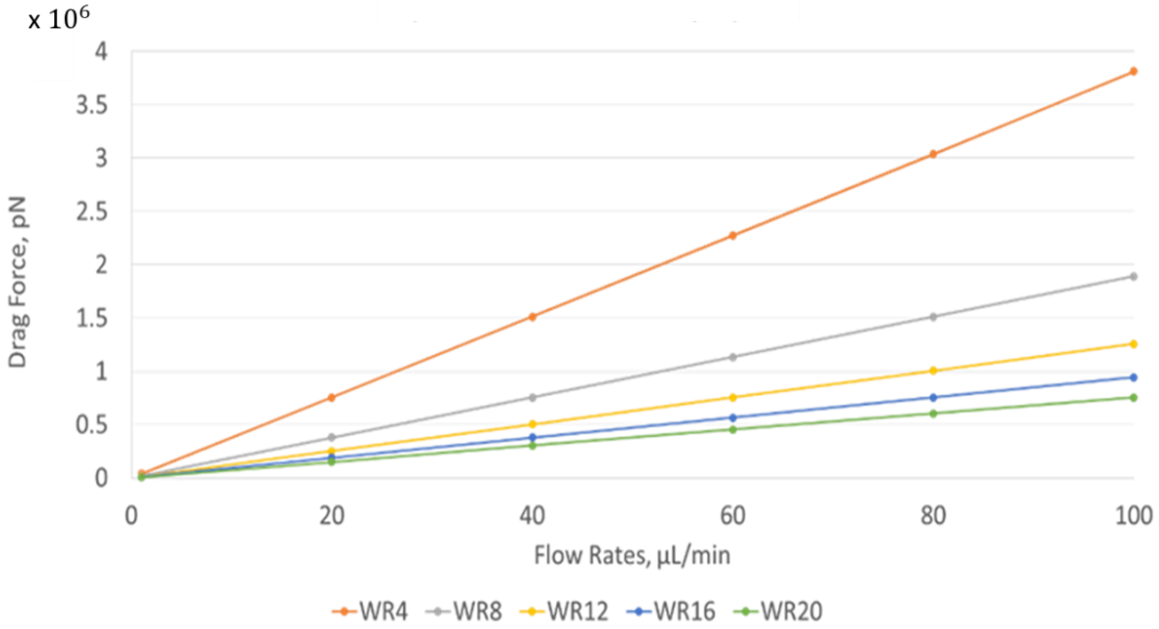

Fig. 7. Relationship between F_{drag} and *Q* at manipulated *WR*

Therefore, it was discovered that at a fixed flow rate and bead size, as the width ratio between the trapping chamber and main channel increases, the drag force decreases. Thus, the highest *WR*, which was 20, causes the lowest drag force between all the microfluidic systems. Apart from that, given that the *WR* and bead size was kept constant, the lowest flow rate of the flowing fluid would produce the lowest drag force. This then concluded that the microfluidic system which caused the lowest drag force, which was, 7.28 x 10^3 pN, was microfluidic channel with trapping chamber with *WR* of 20 and flow rate of 1 µL/min.

In addition, the generated drag force relative to the depth of the *z*-plane of the simulation model was also investigated, as in Figure 8.

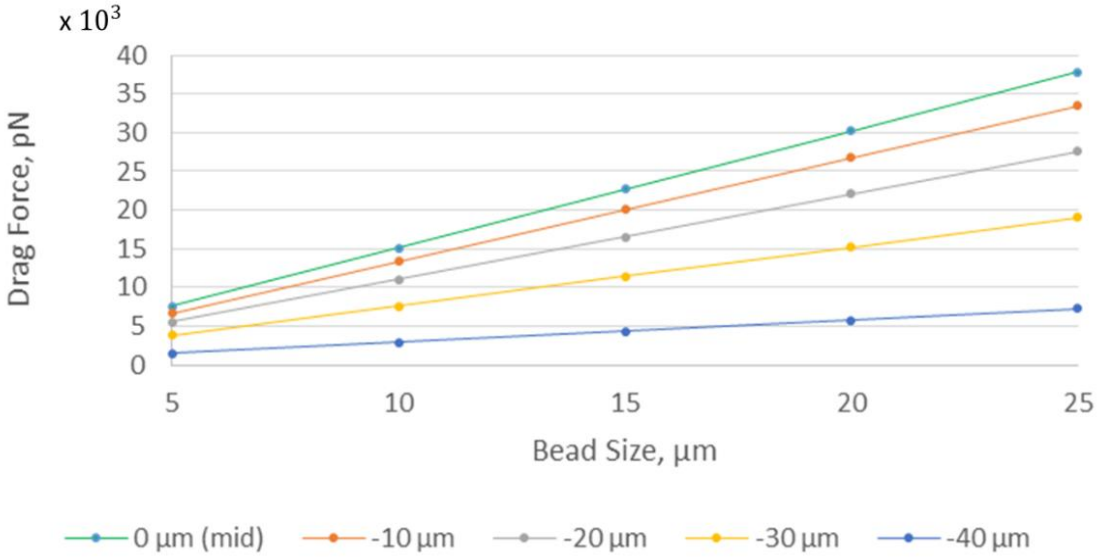

Fig. 8. Relationship between F_{drag} and bead size at manipulated *z*-plane depth

Z-plane with value 0 µm indicated the mid *z*-plane of the microfluidic channel simulation model. Thus, -10 µm corresponded with the plane which was 10 µm from the *z*-axis at the negative side. The bottom wall of the model was located at -50 µm. As can be observed from Figure 8, with bead size of 25 µm, the highest drag force was at the middle of the flowing fluid, which was 3.64 x 10^4 pN, while the lowest generated drag force, 7.24 x 10^3 pN, was observed when it was just 10 µm from the bottom wall. As the flowing fluid was in laminar condition, it followed a parabolic curve of flow, in which the middle of the fluid had the highest velocity, and as the reference point moved away from the middle of fluid, the velocity became lower. Under the condition that there is no magnetic system with reliable magnetic force to high-effectively enable magnetic bead trapping, the magnitudes of velocities according to the *z*-plane depth could be investigated to help studying the trapping efficiency.

Besides that, the relationship between the drag force and the bead size at a constant flow rate was also investigated, as in Figure 9.

As observed in Figure 9, with constant *WR* of 20, when the bead size of 5 µm was applied, the resulting drag force in the trapping chamber was 7.28 x 10^3 pN, while bead size of 25 µm yielded drag force of 3.64 x 10^4 pN for flow rate of 1 µL/min. Oh the other hand, as observed for flow rate of 100 µL/min as in Figure 10, similar pattern of drag force was observed, when the bead size of 5 µm was applied, the resulting drag force in the trapping chamber was 7.36 x 10^5 pN, while bead size of 25 µm yielded drag force of 3.68 x 10^6 pN. Therefore, it was discovered that at a fixed flow rate and width ratio between the trapping chamber and main channel, as the bead size increases, the drag force also increases. This is because higher bead size would have higher volume on which the drag force would act upon.

Therefore, throughout the simulations of 11 different sizes of trapping chamber for the microfluidic channel, the system which produced the lowest drag force was the trapping chamber with *WR* of 20 and flow rate of 1 µL/min. For bead size of 5 µm, drag force of 7.28 x 10^3 pN was generated, while for bead size of 25 µm, the experienced drag force was 3.64 x 10^4 pN. Thus, to enable trapping of magnetic beads, the magnetic force should be higher than the drag force, which was 3.64 x 10^4 pN for the investigated range of bead sizes.

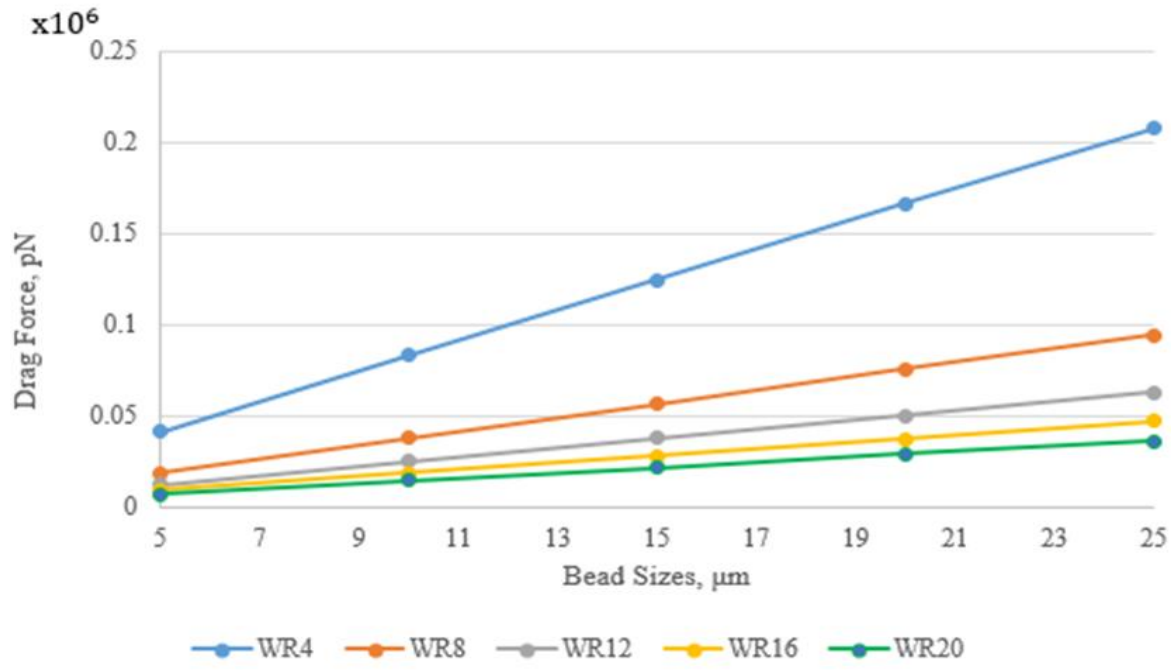

Fig. 9. Relationship between F_{drag} and bead size at Q = 1 µL/min

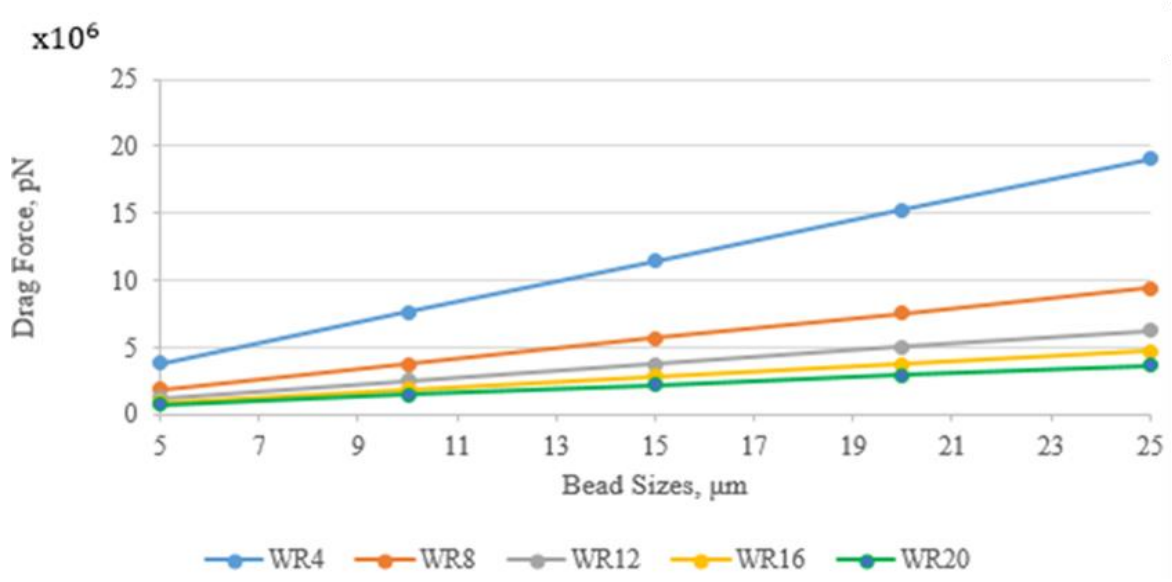

Fig. 10. Relationship between F_{drag} and bead size at Q = 100 µL/min

4.3 Proposal of Magnetic System

In a magnetic-based microfluidic particle trapping system, the trapping of particle will occur when the magnetic force in the trapping chamber is greater than the drag force experienced by the particles. By considering the width ratio between the trapping chamber and main channel of 20 and the volumetric flow rate of 1 µL/min, which produced the lowest drag force, the magnetic force should be greater than 7.28 x 10^3 pN for 5 µm-diameter bead and 3.64 x 10^4 pN for 25 µm-diameter bead. A few magnetic systems utilized by past researchers in their studies were reviewed and summarized, as in Table 3.

Table 3
Magnetic system in past studies

Authors	System	Bead Diameter, µm	Magnetic Force, pN
Derec *et al.,* [21]	Copper conductor in integrated microcircuit	5	14
Ramadan *et al.,* [22]	Circular spiral coil with magnetic pillars	2	2 x 10^3
U. Abidin [1]	Inverted V-shaped nickel ferrite, high gradient electromagnetic system, direct current of 3 Amperes, tip area of 1 μm^2	4.5	3.2 x 10^5

Three different magnetic system which generated different magnitudes of magnetic force were reviewed. Each system generated different range of the magnetic force, which was x10^1, x10^3, and the highest was x10^5 for their respective investigated bead sizes. The microfludic separation magnetic system by A. Ummikalsom, generated magnetic force of 3.2 x 10^5 pN for beads with diameter of 4.5 µm. Under the assumption that the magnetic force would increase as the bead size increases for the range of 5 µm to 25 µm as in this research, the magnetic system by A. Ummikalsom [1] would generate higher magnetic force compared to the produced drag force by the investigated beads in this research. Therefore, inverted V-shaped nickel ferrite, high gradient electromagnetic system with direct current of 3 Amperes and tip area of 1 μm^2 was proposed as the most reliable magnetic system for the microfluidic channel in this research. Further study on the effectiveness of the magnetic systems is to be conducted by future researchers.

5. Conclusion

Study on continuous-flow microbead trapping using microfluidics channel with chamber design has successfully conducted. From the study, as the width ratio between the trapping chamber and main channel increases, the maximum velocity decreases, causing the Reynold's number to decrease. On the other hand, the pressure drop would be larger at higher flow rate. Higher width ratio of trapping chamber and main channel caused reduced drag force value for a constant bead size. At a constant width ratio between the trapping chamber and main channel, larger microbead size contributed to larger drag force. The microfluidic system with *WR* of 20 and flow rate of 1 µL/min produced the lowest drag force, 3.64 x 10^4 pN. Particle trapping would occur when the magnetic force is larger than the drag force. Thus, a high gradient magnetic system is proposed to be used for possible magnetic microbeads trapping in microfluidics continuous flow.

Acknowledgement
This research was funded by a grant from Potential Academic Staff (PAS Q.J130000.2724.02K94) Universiti Teknologi Malaysia.

References
[1] A. Ummikalsom (2016). *High gradient magnetic field lab-on-chip (LOC) for biological cell separation.* (Doctor Philosophy), Universiti Kebangsaan Malaysia, Bangi.
[2] Bhagat, Ali Asgar S., Hansen Bow, Han Wei Hou, Swee Jin Tan, Jongyoon Han, and Chwee Teck Lim. "Microfluidics for cell separation." *Medical & biological engineering & computing* 48, no. 10 (2010): 999-1014.
[3] Plouffe, Brian D., Shashi K. Murthy, and Laura H. Lewis. "Fundamentals and application of magnetic particles in cell isolation and enrichment: a review." *Reports on Progress in Physics* 78, no. 1 (2014): 016601.
[4] Antfolk, Maria, and Thomas Laurell. "Continuous flow microfluidic separation and processing of rare cells and bioparticles found in blood–A review." *Analytica chimica acta*965 (2017): 9-35.
[5] Chen, Yuchao, Peng Li, Po-Hsun Huang, Yuliang Xie, John D. Mai, Lin Wang, Nam-Trung Nguyen, and Tony Jun Huang. "Rare cell isolation and analysis in microfluidics." *Lab on a Chip* 14, no. 4 (2014): 626-645.

[6] Teste, Bruno, Nicolas Jamond, Davide Ferraro, Jean-Louis Viovy, and Laurent Malaquin. "Selective handling of droplets in a microfluidic device using magnetic rails." *Microfluidics and Nanofluidics* 19, no. 1 (2015): 141-153.
[7] Pamme, Nicole, and Claire Wilhelm. "Continuous sorting of magnetic cells via on-chip free-flow magnetophoresis." *Lab on a Chip* 6, no. 8 (2006): 974-980.
[8] Fuerstman, Michael J., Ann Lai, Meghan E. Thurlow, Sergey S. Shevkoplyas, Howard A. Stone, and George M. Whitesides. "The pressure drop along rectangular microchannels containing bubbles." *Lab on a Chip* 7, no. 11 (2007): 1479-1489.
[9] Di Carlo, Dino. "Inertial microfluidics." *Lab on a Chip* 9, no. 21 (2009): 3038-3046.
[10] Hejazian, Majid, Weihua Li, and Nam-Trung Nguyen. "Lab on a chip for continuous-flow magnetic cell separation." *Lab on a Chip* 15, no. 4 (2015): 959-970.
[11] Wu, Wei-Tao, Andrea Blue Martin, Alberto Gandini, Nadine Aubry, Mehrdad Massoudi, and James F. Antaki. "Design of microfluidic channels for magnetic separation of malaria-infected red blood cells." *Microfluidics and nanofluidics* 20, no. 2 (2016): 41.
[12] Gijs, Martin AM, Frederic Lacharme, and Ulrike Lehmann. "Microfluidic applications of magnetic particles for biological analysis and catalysis." *Chemical reviews* 110, no. 3 (2009): 1518-1563.
[13] Qin, Dong, Younan Xia, and George M. Whitesides. "Soft lithography for micro-and nanoscale patterning." *Nature protocols* 5, no. 3 (2010): 491.
[14] Meng, Songdong, Debasish Tripathy, Eugene P. Frenkel, Sanjay Shete, Elizabeth Z. Naftalis, James F. Huth, Peter D. Beitsch *et al.,* "Circulating tumor cells in patients with breast cancer dormancy." *Clinical cancer research* 10, no. 24 (2004): 8152-8162.
[15] Scarberry, Kenneth E., Erin B. Dickerson, Z. John Zhang, Benedict B. Benigno, and John F. McDonald. "Selective removal of ovarian cancer cells from human ascites fluid using magnetic nanoparticles." *Nanomedicine: Nanotechnology, Biology and Medicine* 6, no. 3 (2010): 399-408.
[16] Guide, Fluent User'S. "Version 15, ANSYS." *Inc., April* (2014).
[17] McDonald, J. Cooper, David C. Duffy, Janelle R. Anderson, Daniel T. Chiu, Hongkai Wu, Olivier JA Schueller, and George M. Whitesides. "Fabrication of microfluidic systems in poly (dimethylsiloxane)." *ELECTROPHORESIS: An International Journal* 21, no. 1 (2000): 27-40.
[18] Gorkin, Robert, Jiwoon Park, Jonathan Siegrist, Mary Amasia, Beom Seok Lee, Jong-Myeon Park, Jintae Kim, Hanshin Kim, Marc Madou, and Yoon-Kyoung Cho. "Centrifugal microfluidics for biomedical applications." *Lab on a Chip* 10, no. 14 (2010): 1758-1773.
[19] Neethirajan, Suresh, Isao Kobayashi, Mitsutoshi Nakajima, Dan Wu, Saravanan Nandagopal, and Francis Lin. "Microfluidics for food, agriculture and biosystems industries." *Lab on a Chip* 11, no. 9 (2011): 1574-1586.
[20] Koh, Kai-Seng, Jitkai Chin, Joanna Chia, and Choon-Lai Chiang. "Quantitative studies on PDMS-PDMS interface bonding with piranha solution and its swelling effect." *Micromachines* 3, no. 2 (2012): 427-441.
[21] Derec, Caroline, Claire Wilhelm, Jacques Servais, and Jean-Claude Bacri. "Local control of magnetic objects in microfluidic channels." *Microfluidics and Nanofluidics* 8, no. 1 (2010): 123.
[22] Ramadan, Qasem, Victor Samper, Daniel P. Poenar, and Chen Yu. "An integrated microfluidic platform for magnetic microbeads separation and confinement." *Biosensors and Bioelectronics* 21, no. 9 (2006): 1693-1702.